ACS APPLIED MATERIALS & INTERFACES

Research Article

www.acsami.org

Surface/Interface Carrier-Transport Modulation for Constructing Photon-Alternative Ultraviolet Detectors Based on Self-Bending-Assembled ZnO Nanowires

Zhen Guo,*[,†] Lianqun Zhou,[†] Yuguo Tang,[†] Lin Li,[‡] Zhiqi Zhang,[†] Hongbo Yang,[†] Hanbin Ma,[§] Arokia Nathan,[§] and Dongxu Zhao*[,∥]

[†]CAS Key Lab of Bio-Medical Diagnostics, Suzhou Institute of Biomedical Engineering and Technology, Chinese Academy of Sciences, No. 88, Keling Road, Suzhou New District 215163, People's Republic of China

[‡]Key Laboratory for Photonic and Electronic Bandgap Materials, Ministry of Education, School of Physics and Electronic Engineering, Harbin Normal University, Harbin 150025, People's Republic of China

[§]Department of Engineering, University of Cambridge, Cambridge CB3 0FA, U.K.

[∥]The State Key Laboratory of Luminescence and Applications, Changchun Institute of Optics, Fine Mechanics and Physics, Chinese Academy of Sciences, 3888 East Nan-Hu Road, Open Economic Zone, Changchun 130033, People's Republic of China

Supporting Information

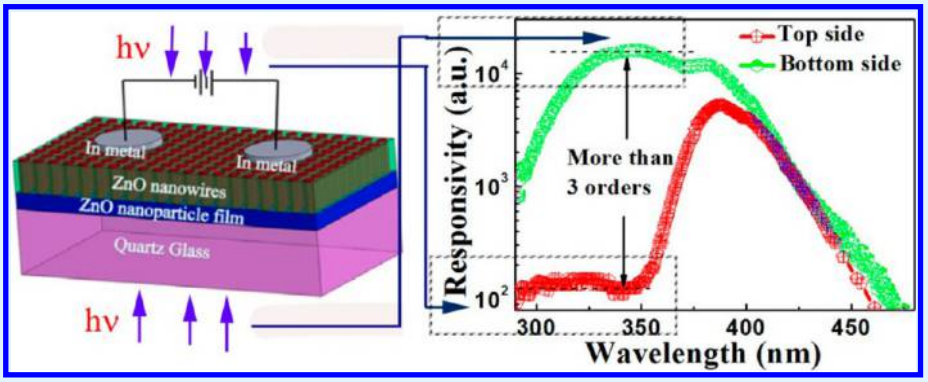

ABSTRACT: Surface/interface charge-carrier generation, diffusion, and recombination/transport modulation are especially important in the construction of photodetectors with high efficiency in the field of nanoscience. In the paper, a kind of ultraviolet (UV) detector is designed based on ZnO nanostructures considering photon-trapping, surface plasmonic resonance (SPR), piezophototronic effects, interface carrier-trapping/transport control, and collection. Through carefully optimized surface/interface carrier-transport modulation, a designed device with detectivity as high as $1.69 \times 10^{16}/1.71 \times 10^{16}$ cm·Hz$^{1/2}$/W irradiating with 380 nm photons under ultralow bias of 0.2 V is realized by alternating nanoparticle/nanowire active layers, respectively, and the designed UV photodetectors show fast and slow recovery processes of 0.27 and 4.52 ms, respectively, which well-satisfy practical needs. Further, it is observed that UV photodetection could be performed within an alternative response by varying correlated key parameters, through efficient surface/interface carrier-transport modulation, spectrally resolved photoresponse of the detector revealing controlled detection in the UV region based on the ZnO nanomaterial, photodetection allowed or limited by varying the active layers, irradiation distance from one of the electrodes, standing states, or electric field. The detailed carrier generation, diffusion, and recombination/transport processes are well illustrated to explain charge-carrier dynamics contributing to the photoresponse behavior.

KEYWORDS: *surface/interface, carrier control, UV photodetection, self-bending assembly, ZnO nanowires*

1. INTRODUCTION

Charge-carrier generation, diffusion, and recombination modulation are all very important considerations in the construction of high-efficiency light-emitting diodes, photodetectors, and solar cells in the field of optoelectronic devices.[1−5] The surface or interface properties of nanomaterials are especially significant to the overall charge-carrier generation, transport, recombination, and/or collection efficiency because the reaction dynamics can be greatly influenced by these properties.[6−9] In the case of applications involving photodetection with high performance, semiconductor nanoparticles and nanowires could be conjugated by taking advantage of their

Received: June 6, 2017
Accepted: August 17, 2017
Published: August 17, 2017

DOI: 10.1021/acsami.7b08066
ACS Appl. Mater. Interfaces 2017, 9, 31042−31053

merits. However, they both have advantages and disadvantages with respect to their photoelectric characteristics. Nanocrystal particles exhibit strong photon absorption productivity for generating carriers in the extended bands, resulting in efficient carrier collection.[10,11] However, a photoelectric device with a channel layer composed of nanoparticles can exhibit unfavorable carrier transport of the generated carriers; the surface/interface trap-modulated hopping and tunneling processes dominate the performance of such devices.[12,13] The photodetectors based on thin films of semiconductor nanocrystal particles demonstrate remarkably high responsivities accompanied by slow responses; meanwhile, large driving voltages are commonly requested.[14] To achieve high gain and low dark current, a large electrode spacing (>5 mm) is needed to allow more photons to be absorbed; the transit time of the charges across the electrodes is correspondingly increased, and the applications of these photodetectors are thus limited.[14−17] By contrast, semiconductor nanowires possess ideal transport characteristics with optimal carrier mobility, exhibiting non-negligible dark current.[18,19] Therefore, during the past decade, nanowire-based ultraviolet (UV) photodetectors have been widely explored, with most efforts focusing on single nanowires or arrays because their merits of high crystal quality and facile fabrication make them suitable for fabricating optoelectronic devices. However, for several reasons, UV photodetector devices based on nanoparticles or nanowires have not shown comparative advantages. Epitaxial single-crystal nanowires have almost no grain boundaries, exhibit much better optoelectronic performances when used in related devices because of the greater carrier diffusion length (>175 μm in single-crystal nanowires, more than 2 orders of magnitude longer than the diffusion length in nanocrystalline thin films), and have a low trap-state density; indeed, a nearly 100% internal quantum efficiency has been achieved in single-crystal nanowire solar cells.[3,20] The photogenerated carriers in single crystals can be completely extracted because of the long carrier diffusion length when the active layer thickness is much larger than that of the thin film, which is highly applicable in photodetection fields. As such, methods to combine the advantages of nanocrystal particles with many grain boundaries and a high density of charge-carrier traps and the advantages of nanowires with excellent crystal quality for carrier transport with high mobility have been developed; efforts to enable good control of charge-carrier transport and trap limitation for building high-efficiency optoelectronic devices are becoming a research hot spot. The issue on how to design photodetectors with low dark current, high detectivity, and quick response utilizing nanoparticle and nanowire structures remains a key challenge. Here, in contrast to these previously reported photodetectors, we developed a UV detector with modulated photoresponse by exploring a vertical structure that combines the low-dark-current noise of nanoparticles and the high mobility of single-crystalline nanowires with adjustable standing states. The active-layer material composed of a free-standing or self-bending assembly of ZnO nanowires and nanoparticles is emerging as a highly applicable nanomaterial because of its high exciton binding energy (60 meV) and wide band gap (3.4 eV) at room temperature.[14,21] ZnO is considered as a low-cost material; it can be prepared by various synthetic strategies and has potential applications in optoelectronic devices.[15,22−24] The preparation of carrier-collection electrodes with ZnO nanowires homoepitaxially grown on a nanoparticle film results in a photoactive layer composed of a ZnO nanocrystal particle film with a thickness of 50 nm and epitaxial single-crystal nanowires longer than 5 μm; these active layers are sufficiently thick for almost all of the UV photons to be completely absorbed. Additionally, to take advantage of the high gain of the photoconductors, at least one of the electrodes is required to be an ohmic contact. ZnO nanowires with free or bending states, when employed as the photoabsorber layer and as high-carrier-mobility electrodes on a ZnO nanoparticle film, can outperform earlier photodetectors because of the application of its nature of ZnO material. Given the piezophototronic effect of ZnO, a vertical-structured photodetector that combines the advantages of nanoparticles and nanowires could be efficiently modified through the design of epitaxial nanowires with changing-standing-states carrier trapping or transport behaviors;[25−27] such a modification would result in a photodetector with an alternative photoresponse. The spectrally resolved photoresponses of the detector reveal photoselective detection in the UV region, which could be well modulated by the photosensitive region, location, electric field, and standing states of the nanowires. The specific UV detectivity as high as $1.69 \times 10^{16}/1.71 \times 10^{16}$ cm·Hz$^{1/2}$/W when illuminated from different locations is realized considering the photon trapping, surface plasmonic resonance (SPR), and piezophototronic effects together. Because of the competition of the surface/interface charge-transport and recombination modulation of the generated carriers, the photoresponse characteristics under different conditions could be well illustrated by the detailed carrier generation, recombination, and diffusion mechanisms, combining the energy-band diagram and charge-carrier dynamics for the contribution of the photoresponse behaviors.

2. RESULTS AND DISCUSSION

ZnO nanoparticles with different sizes of 60, 30, and 15 nm, respectively, were first prepared on quartz glass by the magnetron sputtering method in order to obtain controlled growth of nanowires, as shown in Figure 1a−c; by exploring solution processes, ZnO nanowires can be prepared, assisted by a nanoparticle seed layer in a large scale, as shown in the top scanning electron microscopy (SEM) images in Figure 1d−o, which indicate that the standing states could be well adjusted via changes in the growth conditions; as discussed in the material preparation section, nonbended, less bended, and heavily bended ZnO nanowires with tops aggregated together could be formed by exploring different supporting nanoparticles; through the seed size adjustment of the ZnO nanoparticles, the geometry of the epitaxial nanowires could be efficiently tuned, the aspect ratio for the obtained nanowires could be 38, 63, and 102, and finally the posture of the epitaxial nanowires from vertically aligned to less bended or heavily bended was completely transformed, as shown in the figure, which proves that the seed size plays an important role in tuning the aspect ratio of the nanowires to enable the formation of different standing states by solution processing. Considering photoelectric device fabrication utilizing ZnO nanoparticles and nanowires with controlled morphology, which function as both essential photoactive and/or efficient carrier-transport/trapping layers, combining energy-band and nanosize engineering, it is believed that the corresponding built device performance could be efficiently improved. Here, a schematic diagram of our UV photodetector is presented, as shown in Figure S1 (the corresponding preparation precedure is shown in Figure S2), which explores free-standing or self-bending-assembled ZnO nanowires on a nanoparticle layer as a photoactive layer

DOI: 10.1021/acsami.7b08066
ACS Appl. Mater. Interfaces 2017, 9, 31042−31053

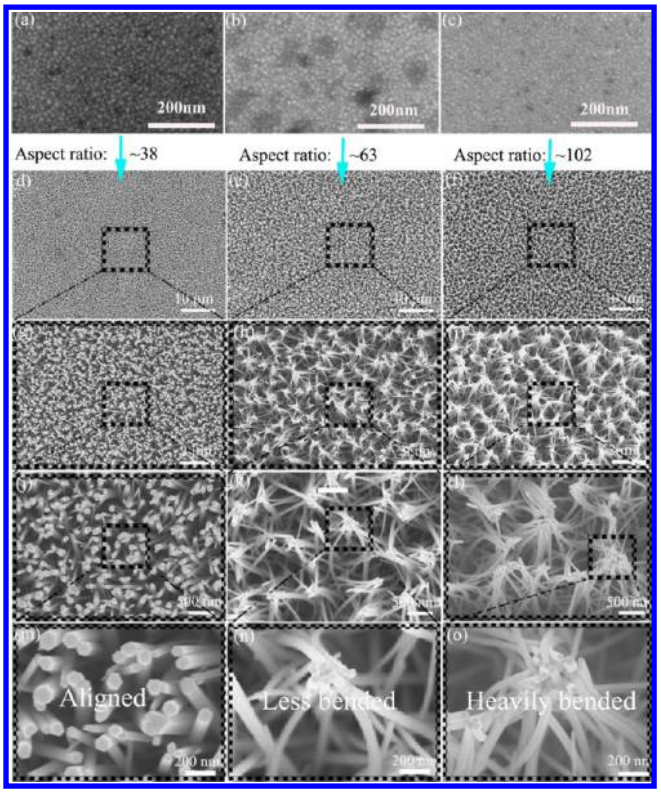

Figure 1. SEM images of nonbended, less bended, and heavily bended ZnO nanowires. (a–c) SEM images of ZnO nanoparticles. (d–o) SEM images of self-assembled ZnO nanowires with free-standing states. The tops of the nanowires display hexagonal morphology with a nonbended state. SEM images of ZnO nanowires with a less bended state. The average amount of nanowires agglomerated together is ~10. SEM images of ZnO nanowires with a heavily bended state. The average amount of nanowires agglomerated together can be ~20.

supported by a quartz glass substrate. The experimental results demonstrate that the UV absorption spectrum was further broadened through the combination of ZnO nanoparticles and nanowires (Figure S3), and the higher-energy UV photons could be efficiently absorbed as a result of the quantum size effect.[28]

As shown in Figure 2a–l, a kind of UV photodetector was designed by considering the key factors such as photon trapping, ZnO–gold (Au) SPR, piezophototronic effects, and energy-band engineering. First, the self-bending-assembled ZnO nanowires mimic the pyramid texture, similar to the antireflection layer of silicon solar cells, as shown in the SEM image from the top view (Figures 2b,c and S4);[29,30] a pyramidal surface texture that causes photon trapping by scattering light into the sensitive region over a large angular range in conventional thick silicon solar cells has been demonstrated to be very efficient for increasing the absorption coefficient in solar cell applications (Figure 2c).[30] Self-bending-assembled ZnO nanowires have long absorption path lengths for photon trapping, especially in high-density nanowire arrays, resulting in carrier collection or transport for efficient carrier extraction.[19] The self-bending-state nanowires with their tops aggregated together increase the effective path length in the framework structure; these nanowires have been demonstrated to be an excellent material for efficient photon trapping, especially in the UV region over a large angular range. Second, to both minimize the dark current and increase the photocurrent, Au nanoparticles were functionalized on the surfaces of the nanoparticles and nanowires. The carriers near the surface of ZnO nanostructures can thus be depleted, and the width of the depletion layer is increased.[31] SPR has been determined to lead to a strong absorption, scattering, and local-field enhancement when the size of plasmonic Au–ZnO nanostructure is less than the incident wavelength, which results in improved UV photodetection.[32,23,32,16] In the present work, through the modification of Au nanoparticles on the surfaces of the ZnO nanostructures, the absorption spectrum is broadened in the visible region, accompanied by an enhanced UV intensity, as shown in Figure S3. The SEM image of Au nanoparticles could be well applied for the surface modification of ZnO nanowires, as shown in Figure 2e. The high-resolution trasmission electron microscopy (HRTEM) image displays the lattice fringes of the Au–ZnO nanostructure interface, from which the interplanar spacing was measured to be 0.260 and 0.235 nm for the ZnO(002) and Au(111) planes shown in Figure 2f, respectively. SPR could be applied here for lowering the dark current while also improving the photocurrent, as shown in the energy-band diagram between the Au and ZnO materials (Figures 2d and S5). Third, as is known, piezophototronic effects could be applied for improving the performance of the photoelectric devices through energy-band-structure modification, as shown in Figure 2g,[33−35] The capillary-force-induced self-bending assembly of ZnO nanowires with tops aggregated together can thus apply piezophototronic effects for the wurtzite structure. The TEM image of the nanowires shows small size variation with an average diameter of ~60 nm (Figure 2i). The detailed TEM image indicates that the tops of the epitaxial nanowires exhibit a nanoneedlelike shape. Meanwhile, in the case of a single nanowire, a uniform size distribution from the root to the neck is observed. The HRTEM image shows that the single-crystal nanowires have lattice fringes perpendicular to the wire axis, which indicates that the epitaxial nanowires grew along the [0001] direction. The equal interplanar distance measured along the nanowire was 2.60 Å, which means that lattice parameter *c* is uniform along the whole nanowire in both the free-standing and bent states. Finally, considering the quantum size effect, the photogenerated carriers in nanoparticles due to their larger band gap compared with nanowires could be easily diffused into nanowires, as shown in the schematic energy-band diagram in Figure 2j; otherwise, there is a barrier layer for blocking carrier transport from nanowires to nanoparticles unless an optimal electric filed is loaded. TEM images of the ZnO nanowires with nanoparticles or dispersed ZnO nanoparticles as the seed layer for the growth of homoepitaxial nanowires are captured in Figure 2k,l, which demonstrate uniform size distribution of the nanowires and nanoparticles, and the homoepitaxial growth mode of the *c*-axis-oriented ZnO nanowires was supported by the same oriented nanocrystal particles.

Interestingly, the photon-alternative response shown in Figure 3a–i was observed in the photocurrent spectra for the detector under UV illumination of 380 nm on self-bending-assembled ZnO nanowires (assigned as the top side) and quartz glass (assigned as the bottom side). A peak appeared at approximately ~380 nm in the photocurrent spectrum when irradiated from the top side; this peak is attributed to the nearby band edge response. The full-width at half-maximum (fwhm) of the photoresponse spectrum is ~34 nm, which means that the response of the photodetector to the photons is limited in a certain spectral range. When UV irradiation was

DOI: 10.1021/acsami.7b08066
ACS Appl. Mater. Interfaces 2017, 9, 31042–31053

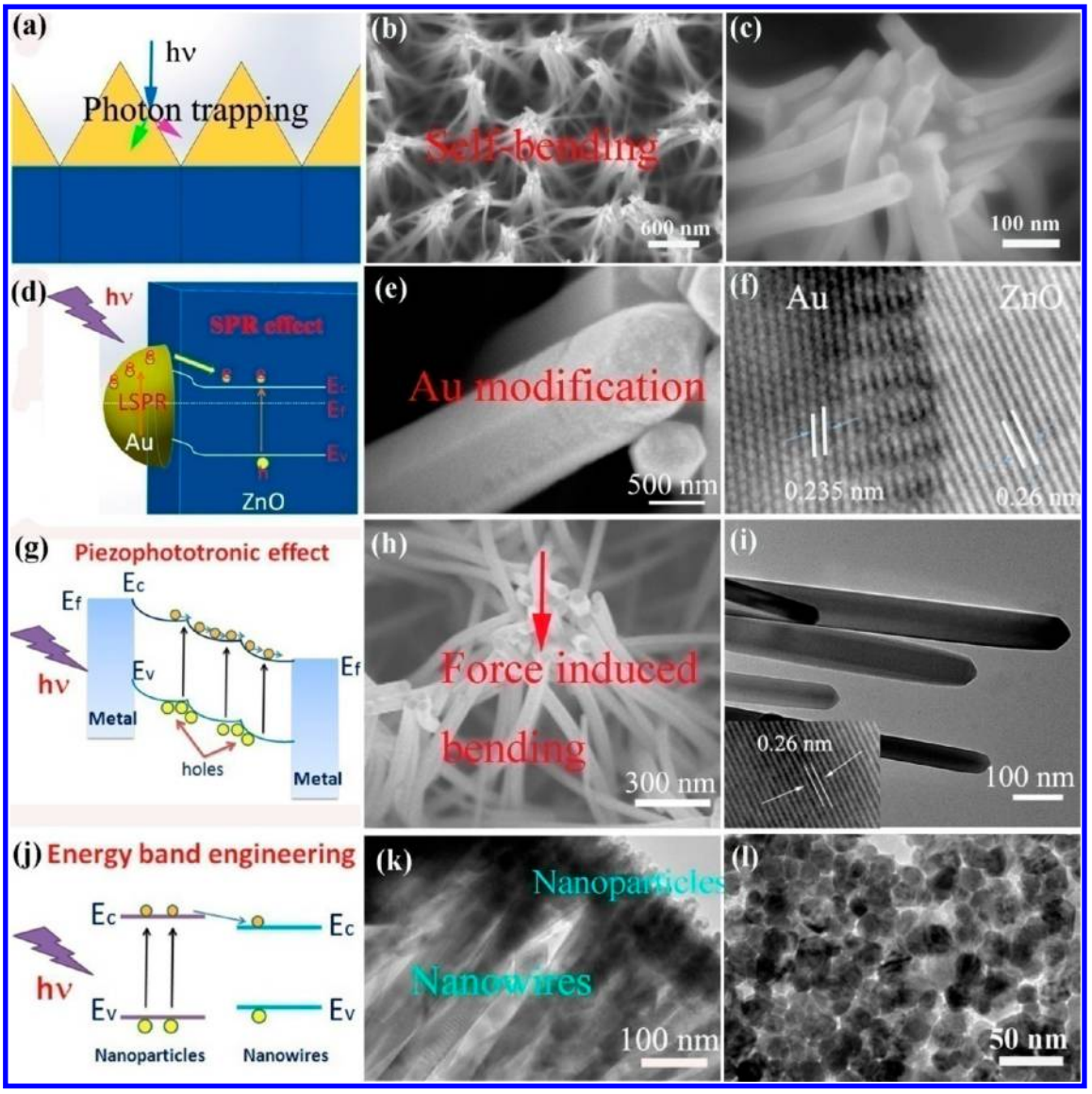

Figure 2. UV photodetector designed by considering the dominant factors such as structure, surface modification, piezophototronic effects, and energy-band engineering. (a) Schematic diagram of photon trapping in the pyramid structure. (b and c) SEM images of self-assembled ZnO nanowires with a tops agglomerated structure, which mimics a typical conventional pyramid structure for efficient photon trapping. (d) Schematic diagram of SPR between Au and ZnO. (e and f) SEM and HRTEM images of ZnO nanowires functionalized with plasmonic Au nanoparticles. (g) Schematic band structure diagram of the ZnO material considering piezophototronic effects. (h) SEM image of self-bending-assembled single-bound ZnO nanowires. (i) TEM and HRTEM images of the ZnO nanowires. (j) Schematic energy-band diagram of ZnO nanowires and nanoparticles, through UV photoexcitation. The generated carriers in the nanoparticles could be easily diffused into nanowires. (k and l) TEM images of ZnO nanowires and nanoparticles.

focused on the bottom side, a new peak appeared at ~350 nm in the shorter-wavelength region. This peak is attributed to the higher-energy absorption-related photoresponse due to the presence of high-energy states.[36] The self-bending-assembled ZnO nanowire photodetector works as follows: first, both active layers of the nanoparticle film and nanowires absorb incident photons and generate photocarriers when illuminated from the bottom with UV light. The excited ZnO nanoparticles inject electrons across the nanoparticle/nanowire interface. The ZnO nanowires then provide photon-injected carriers with a direct pathway to the collection region. While the photodetector is irradiated from the top side, more carriers are generated in the nanowires than in the nanoparticle film, and restricted charge transport over the grain boundaries of the nanoparticles limits effective carrier collection. Because of the efficient carrier trapping among ZnO nanoparticles, the carrier-transport properties of these systems are thus strongly limited in the dark. Under UV photoexcitation, considering the energy-band diagram of nanowires and nanoparticles, the generated carriers in the nanoparticles could be easily diffused into the nanowires; otherwise, there is a barrier layer for blocking carrier transport from the nanowires to nanoparticles unless an optimal electric field is loaded. Nonlinear increases in the free carrier density for the nanoparticles/nanowires irradiated with different wavelengths result in the current becoming strongly interface-limited. This observed characteristic indicates that the proposed photodetector has potential applications in detecting photons with energies within a certain range. The highly selective response mechanisms can also be understood as follows: In the ZnO nanowire/nanoparticle structure, two regions exist in the

DOI: 10.1021/acsami.7b08066
ACS Appl. Mater. Interfaces 2017, 9, 31042−31053

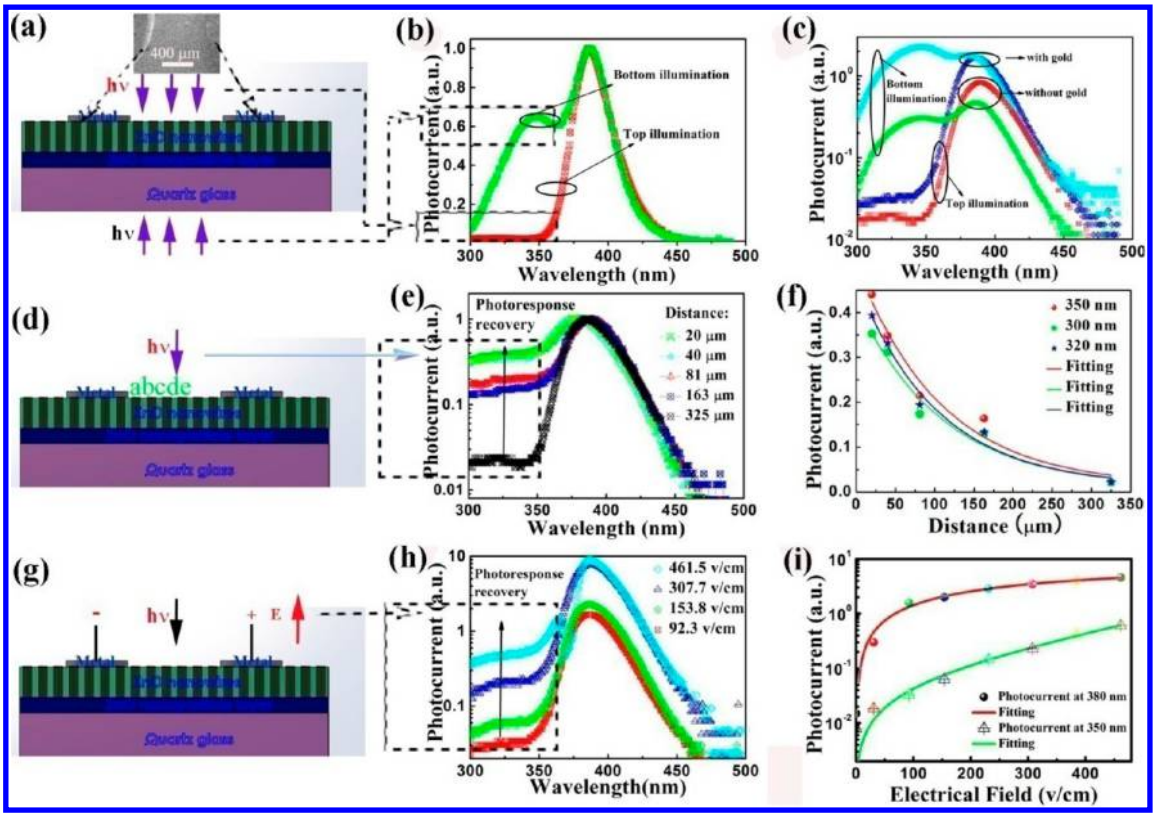

Figure 3. Alternative UV photodetection of ZnO detectors measured while changing the irradiation photoactive layers, the distance from one of the electrodes, and the electric field for exploring photonresponse mechanisms based on as-grown and Au-nanoparticle-modified ZnO nanowire devices. (a, d, and g) Schematic diagrams of a ZnO nanostructure photodetector under UV-light irradiation on the surface of ZnO nanowires or quartz glass side, respectively. (b and c) Photoresponse spectra of self-bending-assembled ZnO photodetectors irradiated from the corresponding locations. The experimental results demonstrate that increased photocurrent was realized after Au modification. (e and f) Photocurrent spectra and analytical data-fitting results of ZnO photodetectors demonstrating exponential decay with increasing distance. (h and i) Photocurrent spectra and analytical data-fitting results of the obtained data located at 350 and 380 nm, respectively, demonstrating exponential growth with increasing electric field.

active layer of the photodetector: a depletion region on the outer layer and a neutral region below the surface. Because a proportional correlation exists between the penetration length and the wavelength, the photons whose energy is greater than the bandgap of ZnO (3.35 eV) will be efficiently absorbed by the depletion region. Nevertheless, under a smaller electric field in the neutral region, the main part of the photogenerated charge carriers cannot reach the depletion region during their lifetime; thus, the photoresponse signal becomes weaker. As a result, the higher-energy photons will be filtered by the neutral region, making the photodetectors highly spectrum-selective.[37] As shown in Figure 3b,c, the photocurrent spectra of the as-grown and Au-nanoparticle-decorated ZnO nanostructures demonstrate that surface modification can remarkably improve the performance of the photodetectors when irradiated on the top or bottom sides, respectively; it can be noted that similar spectral shapes were maintained with increasing photocurrent intensity under the same conditions, which demonstrates that the photoselective detection behavior was not changed. Here, a model based on the energy-band theory is proposed here to provide a better understanding of the enhancement mechanisms, as shown in Figure S5. In the dark, a depletion layer with low conductivity is created near the surface of ZnO by adsorbed oxygen molecule capture of the free electrons on the ZnO surface, and the surface states strongly depend on the Au nanoparticle coverage because of the further increased surface-to-volume ratio after surface modification. Additionally, the materials have different work functions (Au, 5.1 eV; ZnO, 4.1 eV),[38] and the same Fermi energy levels. The charge carriers near the surface of ZnO are depleted by the negatively charged Au nanoparticles, and formation of the increased depletion region is one of the key reasons for decreasing the dark current.[31] Under UV irradiation, the negatively charged oxygen ions are discharged with the photogenerated holes through surface-charge-carrier recombination, and the conductivity of the ZnO device is increased by these photogenerated electrons. Because of hole trapping, the formed barrier at the Au/ZnO interface allows more electrons to be collected. Therefore, the interfaces and the particle-induced scattering for increased light absorption efficiency are responsible for enhancement of the photoresponse.[39] Shown in Figure 3d–f is the mechanism of photoselective detection in the ZnO-nanostructured photodetector by measuring the photocurrent with local irradiation of a light spot at different distances from one of the electrodes, where light irradiation was focused from the top side. The photogenerated carriers were diffused along the bent nanowires, resulting in a weak photocurrent signal upon illumination at the midpoint between electrodes. When the light spot was close enough to one of the electrodes, the generated carriers had sufficient energy to cross the interface barrier via tunneling or thermal emission, resulting in an enhanced shorter-UV-wavelength photoresponse signal for decreasing surface recombination. While the active layer was irradiated in the depletion region or at a location less than a diffusion length

DOI: 10.1021/acsami.7b08066
ACS Appl. Mater. Interfaces 2017, 9, 31042–31053

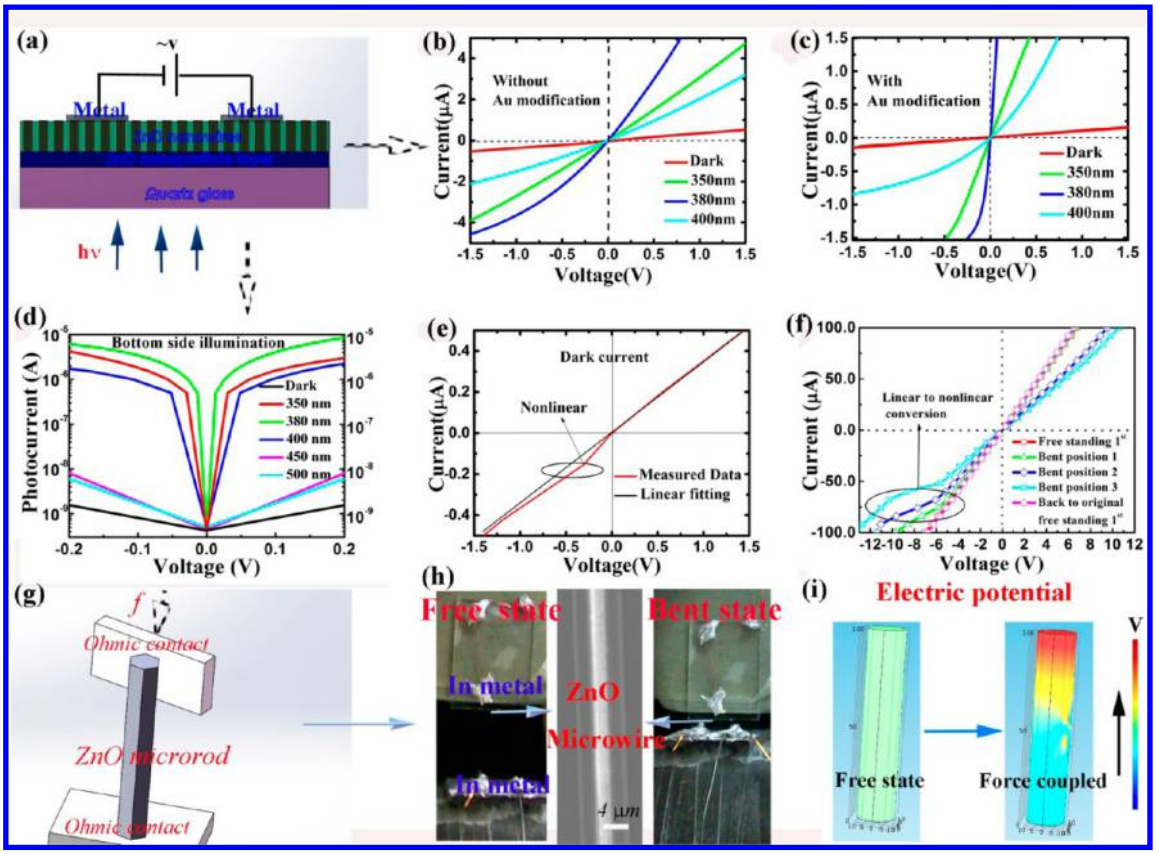

Figure 4. *I*−*V* characteristics of ZnO nanostructure photodetectors explored with and without Au modification, applying force-induced bending and changing the irradiation location. (a) Schematic diagram of the ZnO photodetector. (b and c) *I*−*V* characteristics of the photodetectors without and with Au modification under dark and different irradiation of 350, 380, and 400 nm from the bottom side. (d) *I*−*V* characteristics of the self-bending-assembled ZnO nanowire photodetectors under dark and different illumination wavelengths of 350 and 380 nm and 400, 450, and 500 nm from the top and bottom sides, respectively. (e) Dark-current measurement for a self-bending-assembled ZnO nanowire photodetector. (e and f) *I*−*V* characteristics of a single ZnO microrod with indium metal electrodes under free-standing or bending states. A nonlinear phenomenon occurred under the bending state considering the piezoelectric effect. The *I*−*V* characteristics of the ZnO microrod in the free-standing (from the free-standing first to second indicating the initial and final free-standing states of the ZnO microrod) or different bending states (from bent position 1 to 3 indicating an increase of the bending). (g) Schematic diagram of a single ZnO microrod coupling with force. (h) Experimental setup of a single ZnO microrod under a free or a bent state. (i) Electric potential distribution of a single ZnO microrod under a free or a bent state through theoretical simulation.

away, the local electric field quickly swept away photogenerated electrons and holes in opposite directions from the region. Therefore, the recombination rate was greatly depressed, which greatly enhanced the local conductance. Moreover, the local net charge density in the depletion layer was reduced through migration of the generated carriers. Thus, the local electric field was weakened, resulting in an enhanced photocurrent in the shorter-UV-wavelength region. Through data-fitting analysis, the photocurrents located at 300, 320, and 350 nm show exponential decay with a decay distance factor of ~107 μm^{-1} when the irradiation distance from one of the electrodes is changed. As shown in Figure 3g−i, the strong local electric field quickly swept away the photon-generated carriers from the depletion region at a location less than a diffusion length away, which resulted in a reduced height of the interface barrier for increasing the migration of carriers into the metal electrodes.[40] However, because of the high recombination rate, the contribution of efficiently collected charge carriers for increasing the photocurrent in the center region between the electrodes became much weaker. The electric field dependence of the photocurrent near the electrode contacts varied such that the currents were dominated by electric-field-induced carrier separation. Under larger electric fields, the trapped carriers with higher migration energy will become free with increasing photocurrent. When the electric field was increased from 92.3 to 461.5 V/cm, a shorter-wavelength-region band photocurrent from 300 to 350 nm was enhanced, which demonstrates that the shorter-wavelength response recovery phenomenon under a stronger electric field (Figure 3e) is realized. The dependence of the photocurrent on the electric field and the photoactive layers enables photoselective detection, and the transition of the shorter-UV-wavelength response from low to high was accompanied by a switch of the electric field, reflecting the influence of the majority carrier concentration on the photogenerated carrier recombination rates. The electric-field-dependent photocurrent labeled at 380 and 350 nm exhibited exponential growth with growth constant factors of 418 and 191 cm/V, respectively, which demonstrates efficient carrier injection and collection in the designed ZnO nanostructure photodetector especially under a larger electric field. Meanwhile, considering the influence of factors such as the active layer morphology on the decrease of the shorter-UV-wavelength photocurrent, corresponding experiments were carried out in order to explore detailed response mechanisms utilizing free-standing ZnO nanowires for the design of photodetectors, as shown in Figure S6; enhanced photocurrent could be

DOI: 10.1021/acsami.7b08066
ACS Appl. Mater. Interfaces 2017, 9, 31042−31053

realized based on a self-bending-assembled ZnO nanowire photodetector, and here the specific ratio was given as

$$\mathrm{SR} = P_{\lambda_1}/P_{\lambda_2} \quad (1)$$

where P_λ represents the photocurrent under certain wavelength irradiation. It can be clearly observed that much larger SRs could be realized for a self-bending-assembled ZnO nanowire photodetector, while the photocurrent at the shorter-wavelength range from 300 to 350 nm is maintained in the same level. Experimental results demonstrate that photogenerated carriers could be efficiently collected by the electrodes especially at the shorter UV wavelength, which can be realized and is generally observed in the literature.[23,41] As a piezoelectric material, charge carriers could be trapped by the bending-strain-induced piezopotential, which induced a substantial change in the conductivity of the ZnO nanowires. Because of polarization of the ions, a piezoelectric potential is created in the crystal with noncentral symmetry under the bent state. Hence, charge transport is tuned by the piezopotential, and a channel is created by the local piezoelectric charges via band modification at the interface region.[40,42] For the self-bending-assembled ZnO nanowires, the strain in the wire was mainly axial compressive strain given the capillary-force-induced bending state; in accordance with the studies by Wang et al., the responsivity of the photodetector under compressive strain could be enhanced more than severalfold by introducing strain; notably, the direction of the *c* axis of ZnO will influence the photodetection signal based on single nanowire devices placed in the plane.[42] In our design, vertically aligned ZnO nanowires preferred the (002) *c*-axis orientation, and the generated piezopotential could not switch signs.[40,42]

It is speculated that almost all of the photogenerated carriers could be efficiently collected by electrodes under UV irradiation of different wavelengths on the bottom side based on the experimental results and energy-band diagram of the nanowires and nanoparticles above; here current−voltage (I−V) characteristics were carried out for ZnO nanostructure photodetectors, as shown in Figure 4a−i, and the I−V measurements of the self-bending-assembled ZnO nanowire photodetector devices were carried out without and with Au-nanoparticle modification. Under UV illumination with photon energy greater than the band gap of ZnO, the photocurrent increased greatly compared with the dark current (Figure 4b−d). Because of the local SPR caused by the Au nanoparticles on the surface of the ZnO nanostructures, the dark current decreased and the photocurrent increased, as shown in Figure 4c. The photocurrent for the Au-nanoparticle-modified photodetector increased greatly especially under an irradiation wavelength of 380 nm, which could be due to higher near-band-edge absorption for contributing the photocurrent. Photoexcitation with photon energies greater than the band gap of ZnO could be applied for generating carriers by the higher-energy levels; however, because of the mechanisms discussed in accordance with that mentioned above, the photocurrent becomes a little weaker.[43,44] When the photodetector was irradiated with UV light at a certain position, strong local carrier injection was induced in the area surrounding the light-absorbing ZnO material because of band modification caused by the electric field in the local environment.[14,40] Electrons in ZnO's valence band will be excited into the conduction band under the irradiation of photons with energies greater than the band gap, leaving holes in the valence band. The photocurrent is thus produced by these photogenerated carriers only when they can be efficiently collected by the electrode before recombination occurs. Under top-side UV irradiation with photon energies greater than the band gap of ZnO, the drifting process should dominate transport of the carriers because of an external electric field. Because the external electric field across the nanowire−nanoparticle detector is mainly distributed in the depletion region, photogenerated carriers inside the active layer, especially those generated by the shorter UV wavelengths, are not efficiently collected by the electric field unless the minority carrier diffusion length is large. A strong competition between the carrier recombination and diffusion processes dominates the overall performance of the nanoparticle−nanowire photodetector under different wavelengths for the contribution of nonlinear I−V characteristics. Because of the efficient carrier trapping in the nanostructral device, the dark current of the photodetector under an ultralow driven bias of 0.2 V was as low as 0.7 nA, as shown in Figure 4d; a fast increase of the photocurrent as high as 10 μA is realized under UV irradiation of 380 nm with the same bias. The responsivity can be expressed as

$$R_\lambda = (I_\lambda - I_\mathrm{d})/P_\lambda S \quad (2)$$

where I_λ presents the photocurrent, I_d presents the dark current, P_λ presents the photocurrent, and S presents the effective irradiation area. The calculated R_λ = ~2.605 × 10^5A/W (0.2 V), which is an ultrahigh value obtained under such a very low bias; in other words, a low-cost, high-sensitivity UV detector is designed. According to the equation

$$R_\lambda = q\lambda\eta G/hc \quad (3)$$

where q is elemental charge, λ is the incident wavelength, and η is the quantum efficiency, if η = 1, the photon gain can be G = 8.5 × 10^5, and the obtained detectivity for the top-side irradiation can be expressed as

$$D_\mathrm{T} = R_\lambda/(2qJ_\mathrm{d})^{1/2} \quad (4)$$

The calculated detectivity for the top-side irradiation could be D_T = 1.69 × 10^{16} cm·Hz$^{1/2}$/W (Jones), the detectivity for the bottom-side irradiation D_B = 1.71 × 10^{16} (Jones). J_d is the dark-current density. The quasi-linear I−V characteristics of the ZnO nanostructure photodetector were observed under dark conditions, and the ohmic contact formed between the nanoparticles and homoepitaxial nanowires was used to gain high detectivity of the photoconductors.[23] Actually, the nonlinear I−V characteristics with a nonsymmetric curve at voltages below ±1.5 V, as shown in Figure 4e, demonstrate that a certain electric potential actually existed in the ZnO nanostructural photodetector. Further experimental results prove that the bending of a single ZnO microwire by an external force could cause transformation of the I−V characteristics from linear to nonlinear considering the piezoelectric effect. The experimental results and theoretical simulation demonstrate that nonlinear I−V characteristics could be due to the electric potential resulting from piezoelectric effects, as shown in Figure 4f−i, and the asymmetric change of the I−V curve under certain bias, in our case, is dominated by the piezoelectric effect for the ZnO microwire, which tends to shift the height of the local interface barrier at the metal−ZnO contact; while photoexcitation uses light that has an energy higher than that of the band gap of ZnO, the barrier height could be tuned by piezophototronic effects.[40] Also, the photoresponse mechanisms for the ZnO

DOI: 10.1021/acsami.7b08066
ACS Appl. Mater. Interfaces 2017, 9, 31042−31053

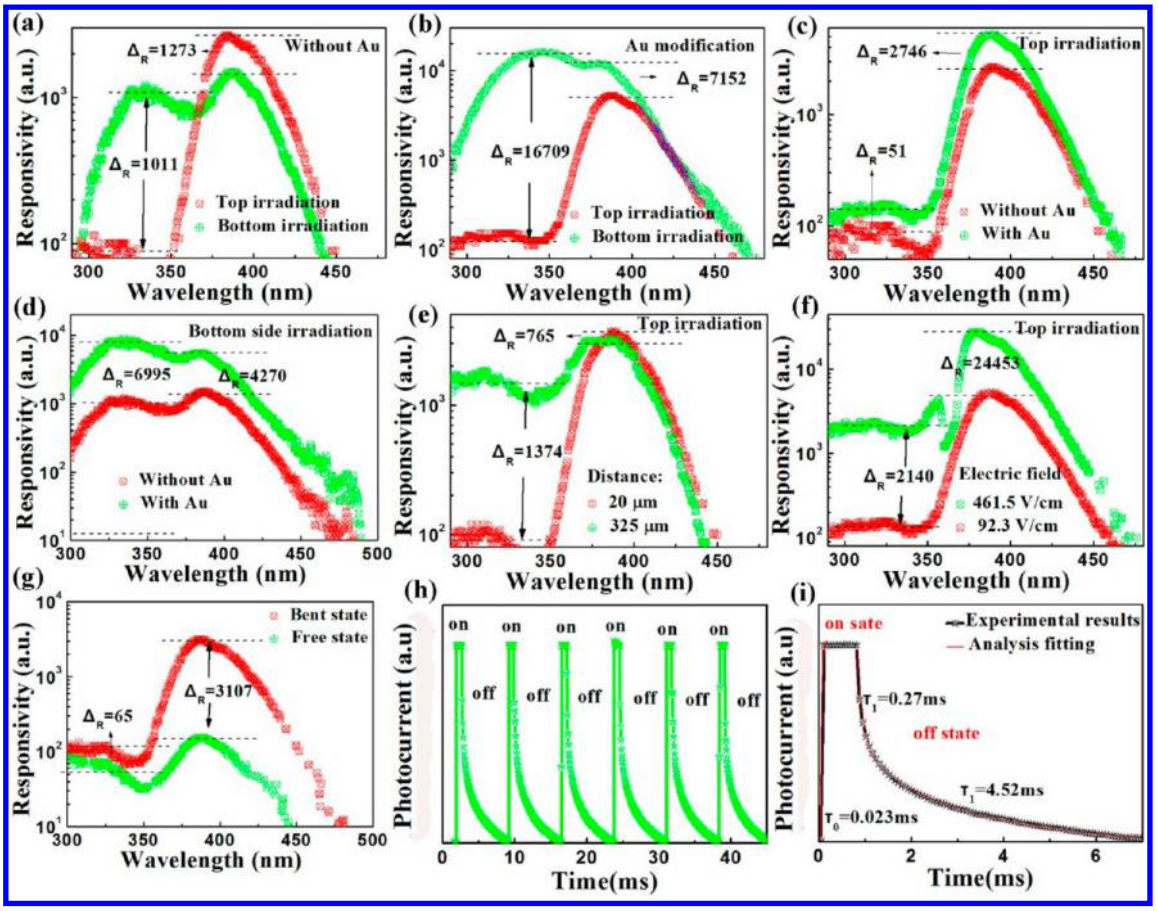

Figure 5. Performance evaluation of the designed ZnO UV photodetectors while changing the corresponding parameters such as irradiation photoactive layers, Au modification, distance, electric field, and nanowire standing state, which shows correlations for the ZnO nanowire devices. (a–g) Responsivity spectra of the ZnO nanostructure photodetector while varying the corresponding parameters, respectively. (h and i) Time-resolved photocurrent of the designed self-bending-assembled ZnO nanowire photodetectors under UV on and off states.

material are commonly explained on the basis of the surface absorption and desorption of oxygen on the nanostructure. Because oxygen molecules are easily adsorbed onto the oxide surface because of the surface traps, the free electrons can be captured by the adsorption of oxygen to generate electronegative oxygen; a low-conductivity layer is then formed near the surface. Upon illumination with photons with energies greater than the band gap of ZnO, photogenerated carriers are generated. The holes can be trapped near the semiconductor surface by the adsorbed electronegative oxygen. This hole-trapping mechanism through oxygen adsorption and desorption in ZnO is affected by the density of trap states formed by the dangling bonds on the nanostructure surface. Any detrimental recombination that occurs at the surface will reduce the magnitude of the photocurrent. Combining the effects such as photon trapping, SPR, and piezophototronic effects together for modulating the carrier transport, the combination of the low dark current and large gain of the photoresponse is expected to yield a type of photodetector with the capability of a photodetector to detect the much weaker light signal.[14]

Given the photoresponse mechanisms of the self-bending-assembled ZnO nanowire photodetector, surface-charge recombination is a possible mechanism for the narrow spectral photoresponse because of the numerous surface/interface-related phenomena observed in the nanostructures. Because of the high-density dangling bonds and quick charge recombination allocated to the nanostructure surface-enhanced visible photoluminescence (PL) emission,[45] high densities of surface-charge traps were observed in the ZnO nanostructures, which explains the large photoconductive gain in the ZnO photodetectors. Actually, the solution-processed ZnO nanowires are unlikely to be free of surface defects. The surfaces will be contaminated through the attachment of nonstoichiometric precursors when the nanowires are removed from the precursor solution. An unavoidable surface-charge recombination, especially for the self-bending-assembled ZnO nanostructure photodetector, as shown in Figure S7, and strong UV emission located at ∼380 nm (near-band-gap recombination) accompanied by nonnegligible visible emission around 550 nm (surface-charge-related recombination) could be clearly observed, which may be considered as one of the key factors enabling narrow-band photodetection. It is also noted that the band gap of ZnO could be modified under local strain, which could induce light emission changes, as reported by Liao et al.[46−48] Through a comparison of the PL emissions of the bending and free-standing state nanowires, enhanced UV emission accompanied by a slight peak shift was observed for bending state nanowires; here, crystal-symmetry modification for contributing luminescence changes under strain is one of the influencing factors. Because of the very large absorption coefficient of the ZnO nanowire materials with photon energies greater than the band gap, the light penetration depth was very small (<370 nm); thus, most of the charge carriers were generated in a narrow region near the electrode, as illustrated in

DOI: 10.1021/acsami.7b08066
ACS Appl. Mater. Interfaces 2017, 9, 31042−31053

Table 1. Comparison of the Alphabet of Lines, Detectivity, Dark Current, Recovery Time between the Present Photodetectors and Previously Reported Ones

photodetector	response type	detectivity (Jones)	dark current	recovery time	ref
ZnO nanowire	non-photon-alternative	3.3×10^{17} (1 V, 365 nm)	20 pA	0.32 s	21
colloidal ZnO nanoparticle	non-photon-alternative		<120 pA/120 V	1 s	15
graphene−quantum dot	non-photon-alternative	7×10^{13}			50
perovskite single crystal	non-photon-alternative	2×10^{10} (570 nm)	nA	∼ms	45
n-ZnO/p-NiO core−shell nanowire	non-photon-alternative			10.0 and 30.3 μs	51
self-bending-assembled ZnO nanowire	photon-alternative	$1.69 \times 10^{16}/1.7 \times 10^{16}$ (0.2 V, 380 nm)	∼1 nA (0.2 V)	growth, 0.023 ms; decay 1, 0.47 ms; decay 2, 4.52 ms	present work

the irradiation-location-dependent photocurrent spectra. Under the above band-gap photoexcitation, the generated charge carriers can be quenched easily because of the severe surface-charge recombination. Surface recombination may dominate the shorter UV photoresponse for the ZnO nanostructure detector.[49] In addition, the surface-charge sinks can quickly trap photogenerated charge carriers near the nanostructure surface. The shorter-UV-wavelength photoresponse inhibition is therefore supported because of the surface-charge-carrier recombination. Photons with energy approaching the band-gap energy penetrate much deeper because of their much higher absorption coefficients. Under the external electric field, these photogenerated charge carriers are driven toward the electrode before recombination; thus, the charge collection efficiency is increased. Therefore, a stronger photoresponse signal in the longer-UV-wavelength range is realized, resulting in the observed peak in the photocurrent spectra. However, with increasing electric field strength, the charge extraction efficiency was further improved, and the photocurrent for the shorter-UV-wavelength range increased much more rapidly. This type of photodetector device lost its narrow-band-detection capability under an electric field greater than 300 V/cm. A larger electric field quickly pushes the photogenerated carriers away from the surfaces, contributing to the generation of photocurrent before recombination. The photocurrent variation induced by a changing electric field can again be explained by the presence of surface modification. However, the applied electric field should not be too large for narrow-band photodetection.[45] The nanocrystal particle interfaces between the crystalline domains that make up the semiconductor photodetector are also critical for efficient charge-transport control.[7] Transport within these domains, as well as at their boundaries, requires attention and optimization.[29] When interface barriers are formed among ZnO nanocrystal particle interfaces under irradiation with photon energies larger than the band gap, electrons in the valence band of ZnO are excited into the conduction band and strong local electric fields are formed in the depletion region;[40] the current is generated only when these photogenerated charge carriers can drift or diffuse to the electrode before recombination. Under light irradiation at the depletion region or at a location less than a diffusion length away, the photogenerated electrons and holes are quickly swept away in opposite directions by the strong local electric field. Therefore, the local conductance is greatly enhanced, followed by a depressed recombination rate. The local net charge density is decreased with migration of the photogenerated carriers into the depletion layer, and the local electric field is diminished. In addition, factors such as the vacuum, temperature, and humidity should also be considered for the photoresponse signal contribution, which may cause adsorption/desorption of environmental molecules on the nanostructure surfaces or affect the carrier-transport properties, resulting in changes for photoresponse behaviors. Also, in our measurement process, all of the experiments were carried out under constant ambient conditions, and these aforementioned influences are much weaker from one or another photodetector.

To evaluate the overall performance of the designed ZnO nanowire UV photodetectors, responsivity spectral measurements were carried out while changing the corresponding parameters such as irradiation photoactive layers, Au modification, distance, electric field, and nanowire standing state, and correlations could be clearly made for clarifying specially constructed UV detectors compared with the generally built ones, as shown in Figure 5a−g. Through careful checking of the responsivity spectra of the ZnO nanostructure photodetector while varying the corresponding parameters, the photon-alternative detection or response output signal intensity could be well modulated through surface/interface carrier-transport control. Here, in order to compare the differentials of the device under different conditions, the photoresponsivity difference Δ_R was given as

$$\Delta_R = R_{\max,\lambda} - R_{\min,\lambda} \quad (5)$$

where $R_{\max,\lambda}$ and $R_{\min,\lambda}$ represent the maximum and minmum responsivities under certain wavelengths for the detectors. Through the overall measurement of the designed detectors, the folowing conclusions can be reached: (1) as shown in Figure 5a,b, more than 3 orders of enhancement for Δ_R could be realized in the spectra ranging from 325 to 350 nm after Au modification based on a self-bending-assembled ZnO nanowire photodetector, which demonstrates an ultrahigh specific ratio as a photon-alternative detector; (2) only the responsivity enhancement (more than 2 orders) located around 380 nm was observed without modifying the alphabet of lines for the spectra (Figure 5c,d); (3) in accordance with literature results, higher responsivity could be realized by varying the irradiation distance or larger electric field, which proves that photogenerated carriers could be efficiently collected before recombination in a region less than the diffusion length or under larger electric field,[21,42] and shorter-UV-wavelength response can be recoverd; (4) through a comparison of the responsivities of the nanowire photodetectors by utilizing vertically aligned or self-bending states, enhanced responsivity (more than 2 orders) could be clearly observed. Meanwhile, the photoresponse speed is commonly measured as a dominant

DOI: 10.1021/acsami.7b08066
ACS Appl. Mater. Interfaces 2017, 9, 31042−31053

parameter for practical applications; under a chopper-generated short-light-pulse signal, the response time of the designed ZnO nanostructure photodetectors could be applied for repeated measurement, and fast and slow recovery processes of 0.27 and 4.52 ms for the nanowire device could be realized, as shown in Figure 5h,i, respectively. The self-bending-assembled ZnO nanowires modified with Au nanoparticles with very high carrier mobility increase the effective diffusion and dominated the rapid recovery rate, and the surface/interface states in the ZnO nanostructures contribute a key role for the slow process.[25] At present, none of the articles have fully explored the detailed mechanisms of the UV photodetectors based on self-bending-assembled ZnO nanowires, which could be well modulated as discussed above; only a few research papers have reported narrow band photoresponse behavior based on the built structure; here, in order to compare specialty differences with others, only a few literatures related with photodetectors due to narrow-band response behaviors were cited, as shown in Table 1; by a comparison of the parameters of the present and previously reported ones, it can be clearly observed that the built device due to ultrahigh detectivity and modulated photoresponse behavior could be realized under ultralow bias of 0.2 V. As such, a kind of UV photodetector with modulated photoresponse could be realized through surface/interface carrier-transport control, and excellent performance of ultrahigh detectivity photodetector under ultralow bias with specific spectrum detection and fast response time could be constructed, which satisfies the practical needs for low power consumption and high sensitivity applications especially in the UV region.[14]

3. CONCLUSION

In conclusion, the designed device with detectivity as high as $1.69 \times 10^{16}/1.71 \times 10^{16}$ cm·Hz$^{1/2}$ /W irradiated with 380 nm photons under ultralow bias of 0.2 V by alternating photoactive layers was obtained with consideration of photon-trapping, SPR, piezophototronic effect, and energy-band engineering, respectively. A kind of modulated UV photodetector was realized through surface/interface carrier-transport control based on self-bending-assembled ZnO nanowires. UV photodetection could be performed within a narrow band by varying correlated key parameters, with respect to efficient carrier trapping or transport control, spectrally resolved photoresponses of the detector revealed photoselective detection in the UV region for contributing detected signal. It is believed that carriers could be efficiently controlled by the surface/interface states of the self-bending-assembled ZnO nanowires, and photon-alternative detection was allowed or limited by the photoactive layers, diffusion length, piezophototronic effects, and electric field. Because of the efficient carrier trapping/transport among ZnO nanostructural devices, the carrier-transport properties of these systems were strongly limited or allowed in the dark or UV photon irradiation. Therefore, the photoresponse of the selective wavelength band resulted from effective carrier generation, separation, and transport, which could be effectively modulated through optimal structure design. The response time of the photodetector showed a rise or decay time on the order of milliseconds, which satisfies the practical needs of such a device. Hence, a high-performance UV photodetector with both high sensitivity and quick response speed is realized through modulation of the contribution of the surface/interface carrier-transport mechanisms. More importantly, the idea of exploration of the constructed device in the paper could also be applied for the design of photoelectric devices especially in the nano research field considering surface/interface carrier-transport properties in the visible or IR region with improved performance.

4. EXPERIMENTAL METHODS

Material Preparation. For ZnO nanowires, first the ZnO nanoparticle films were prepared by the radio-frequency (RF) magnetron sputtering method using a 99.999% pure ZnO target. Before being loaded into the sputtering chamber, the quartz glass substrate was cleaned by organic solvents, a sulfuric acid/hydrogen peroxide mixture, and rinsed by deionized water to remove any contaminants. During the sputtering process, a mixed gas of oxygen and argon with the same flow rate of 20 standard cubic centimeters per minute (SCCM) was introduced into the chamber, and the working pressure was maintained at 1 Pa. The substrate was kept at room temperature with a rotation speed of 20 loops/min. The nanoparticle size of the supporting seed layers could be tuned by a postannealing process, growth time, and buffer layers. Then a solution-processed hydrothermal method was explored to grow homoepitaxial nanowires on the ZnO nanoparticle film using $Zn(CH_3COO)_2{\cdot}2H_2O$ and $C_6H_{12}N_4$ as reactant sources. The reaction solutions were adjusted to identical concentrations (0.01 mol/L). Then the reaction kettle was placed in an oven and maintained at 90 °C. Finally, the obtained sample was rinsed by deionized water and dried in the oven. Standing states of the ZnO nanowires could be well tuned by exploring supporting seed layers or a postgrowth process exploring a liquid solution.

For ZnO microwires with lengths up to several centemeters, a simple one-step chemical vapor deposition method was carried out to prepare ZnO microwires using a furnace tube, using a mixture of ZnO and graphite powders with a weight ratio of 1:1 as the reactant source material. A silicon substrate with a ZnO thin film as the seed layer (deposited via a RF magnetron sputtering method) was utilized as a target. The tube furnace was heated to 1200 °C at a rate of 25 °C/min under a constant flow of argon (160 SCCM) as the protecting gas. After being maintained at 1200 °C for 1 h until the reaction was complete to obtain microwires with lengths as long as possible, the furnace was cooled to room temperature naturally. Then, the ZnO microwires with lengths up to several centemeters could be synthesized on the substrate.

Device Fabrication. For a ZnO nanowire photodetector: to make photodetectors, a poly(methyl methacrylate) (PMMA) resist was used as an insulating transparent filling material for the interspace of the free-standing or bending state nanowires, and oxygen plasma was explored to make the tops of the nanowires uncovered for metal electrode preparation; then oxygen plasma was applied for a second time to make the surfaces of the ZnO nanowires fully uncovered by the PMMA resist. Metal electrodes on the tops of ZnO nanowires were explored as ohmic contacts. Here, the homoepitaxial quasi-single-crystal ZnO nanowires could be regarded as both photoactive layers and vertical electrodes for photodetectors because of an ultrahigh diffusion length of more than 100 μm. The surfaces of the obtained nanowires could be modified by partial coverage of the metal nanoparticles in order to enhance the performances of the photodetectors. Here, Au nanoparticles were deposited on the surface of the ZnO nanowires for metal modification using an ion-sputtering method.

For a single ZnO microwire device: to fabricate a single microwire device applied for piezoelectric effect measurement, a single ZnO microwire with a length up to 3 cm was selected. Both ends of the microwire were contacted with indium metal deposited on a flexible poly(ethylene terephthalate) substrate as electrodes. Bending experiments of a single microwire device could be carried out by an external force using a mechnical displacement fixture with a minmum precision of ± 0.5 μm.

Appratus Applied. SEM images were captured by a Hitachi S-4800 microscope, and PL measurements were obtained using a JY-630 micro-Raman spectrometer with the 325 nm line of a helium–

DOI: 10.1021/acsami.7b08066
ACS Appl. Mater. Interfaces 2017, 9, 31042–31053

cadmium laser as the excitation source. The photocurrent spectra of the devices were detected by a standard lock-in technique with a 150 W xenon lamp as the excitation light source. *I*−*V* measurement was performed by a Lakeshore 7707 Hall measurement system. The UV−vis absorption spectra were recorded on a PerkinElmer Lamda950 spectrophotometer. X-ray diffraction was performed using a Bruker Advance D8 X-ray diffractometer. TEM measurements were performed with an FEI Tecnai G220 instrument.

■ ASSOCIATED CONTENT

Supporting Information

The Supporting Information is available free of charge on the ACS Publications website at DOI: 10.1021/acsami.7b08066.

Schematic diagram of the ZnO nanowire photodetector, ZnO nanostructure photodetector fabrication processes, absorption spectra of the ZnO structure, schematic diagram and SEM image of the pyramid structure, schematic diagram of ZnO with and without Au modification in the dark and under UV light on and off states, photocurrent spectra of ZnO detectors utilizing nanowires with a vertically aligned or a self-bending-assembled structure, PL spectra of bending and free-standing state ZnO nanowires, and mechanism of narrow-band photodetection (PDF)

■ AUTHOR INFORMATION

Corresponding Authors

*E-mail: guozhen@sibet.ac.cn (Z.G.).
*E-mail: zhaodx@ciomp.ac.cn (D.Z.).

ORCID

Zhen Guo: 0000-0002-1647-7239

Author Contributions

The manuscript was written through contributions of all authors. All authors have given approval to the final version of the manuscript.

Notes

The authors declare no competing financial interest.

■ ACKNOWLEDGMENTS

This work is supported by the National Natural Science Foundation of China (Grants 51202154, 51675517, and 51205268), the Natural Science Foundation of Jiangsu Province (Grants BK20131169, BK20160057, and BK2012190), Youth Innovation Promotion Association CAS (No. 2014280), Major Technology Innovation Projects of Jiangsu Province (Project BO2015007), the Key Research Program of the Chinese Academy of Sciences (Grant KFZD-SW-204), the National Key Instrument Developing Project of China (Grant ZDYZ2013-1), and the SRF for ROCS, SEM, and the project funded by the China Postdoctoral Science Foundation (Grant 2016M601890).

■ REFERENCES

(1) Simon, J.; Protasenko, V.; Lian, C. X.; Xing, H. L.; Jena, D. Polarization-Induced Hole Doping in Wide-Band-Gap Uniaxial Semiconductor Heterostructures. *Science* **2010**, *327*, 60−64.

(2) Uoyama, H.; Goushi, K.; Shizu, K.; Nomura, H.; Adachi, C. Highly Efficient Organic Light-Emitting Diodes from Delayed Fluorescence. *Nature* **2012**, *492*, 234−238.

(3) Shi, D.; Adinolfi, V.; Comin, R.; Yuan, M. J.; Alarousu, E.; Buin, A.; Chen, Y.; Hoogland, S.; Rothenberger, A.; Katsiev, K.; Losovyj, Y.; Zhang, X.; Dowben, P. A.; Mohammed, O. F.; Sargent, E. H.; Bakr, O. M. Low Trap-State Density and Long Carrier Diffusion in Organolead Trihalide Perovskite Single Crystals. *Science* **2015**, *347*, 519−522.

(4) Xing, G. C.; Mathews, N.; Sun, S. Y.; Lim, S. S.; Lam, Y. M.; Gratzel, M.; Mhaisalkar, S.; Sum, T. C. Long-Range Balanced Electron- and Hole-Transport Lengths in Organic-Inorganic Ch3nh3pbi3. *Science* **2013**, *342*, 344−347.

(5) Polman, A.; Knight, M.; Garnett, E. C.; Ehrler, B.; Sinke, W. C. Photovoltaic Materials: Present Efficiencies and Future Challenges. *Science* **2016**, *352*, aad4424.

(6) Hwang, Y. J.; Hahn, C.; Liu, B.; Yang, P. D. Photoelectrochemical Properties of TiO2 Nanowire Arrays: A Study of the Dependence on Length and Atomic Layer Deposition Coating. *ACS Nano* **2012**, *6*, 5060−5069.

(7) Graetzel, M.; Janssen, R. A. J.; Mitzi, D. B.; Sargent, E. H. Materials Interface Engineering for Solution-processed Photovoltaics. *Nature* **2012**, *488*, 304−312.

(8) Nakano, M.; Shibuya, K.; Okuyama, D.; Hatano, T.; Ono, S.; Kawasaki, M.; Iwasa, Y.; Tokura, Y. Collective Bulk Carrier Delocalization Driven by Electrostatic Surface Charge Accumulation. *Nature* **2012**, *487*, 459−462.

(9) Fu, X. W.; Liao, Z. M.; Xu, J.; Wu, X. S.; Guo, W. L.; Yu, D. P. Improvement of Ultraviolet Photoresponse of Bent ZnO Microwires by Coupling Piezoelectric and Surface Oxygen Adsorption/Desorption Effects. *Nanoscale* **2013**, *5*, 916−920.

(10) Tsang, M. K.; Bai, G. X.; Hao, J. H. Stimuli Responsive Upconversion Luminescence Nanomaterials and Films for Various Applications. *Chem. Soc. Rev.* **2015**, *44*, 1585−1607.

(11) Wan, D. H.; Chen, H. L.; Tseng, T. C.; Fang, C. Y.; Lai, Y. S.; Yeh, F. Y. Antireflective Nanoparticle Arrays Enhance the Efficiency of Silicon Solar Cells. *Adv. Funct. Mater.* **2010**, *20*, 3064−3075.

(12) McCold, C. E.; Fu, Q.; Howe, J. Y.; Hihath, J. Conductance Based Characterization of Structure and Hopping Site Density in 2d Molecule-Nanoparticle Arrays. *Nanoscale* **2015**, *7*, 14937−14945.

(13) Li, K. Y.; Shan, Q. S.; Zhu, R. P.; Yin, H.; Lin, Y. Y.; Wang, L. Q. Carrier Transport in Quantum Dot Quantum Well Microstructures of the Self-Assembled Cdte/Cds/Ligand Core-Shell System. *Nanoscale* **2015**, *7*, 7906−7914.

(14) Guo, F. W.; Yang, B.; Yuan, Y. B.; Xiao, Z. G.; Dong, Q. F.; Bi, Y.; Huang, J. S. A Nanocomposite Ultraviolet Photodetector Based on Interfacial Trap-Controlled Charge Injection. *Nat. Nanotechnol.* **2012**, *7*, 798−802.

(15) Jin, Y. Z.; Wang, J. P.; Sun, B. Q.; Blakesley, J. C.; Greenham, N. C. Solution-Processed Ultraviolet Photodetedtors Based on Colloidal ZnO Nanoparticles. *Nano Lett.* **2008**, *8*, 1649−1653.

(16) Konstantatos, G.; Howard, I.; Fischer, A.; Hoogland, S.; Clifford, J.; Klem, E.; Levina, L.; Sargent, E. H. Ultrasensitive Solution-Cast Quantum Dot Photodetectors. *Nature* **2006**, *442*, 180−183.

(17) Konstantatos, G.; Sargent, E. H. Nanostructured Materials for Photon Detection. *Nat. Nanotechnol.* **2010**, *5*, 391−400.

(18) Seong, H.; Yun, J.; Jun, J. H.; Cho, K.; Kim, S. The Transfer of Charge Carriers Photogenerated in ZnO Nanoparticles into a Single ZnO Nanowire. *Nanotechnology* **2009**, *20*, 245201.

(19) Hochbaum, A. I.; Yang, P. D. Semiconductor Nanowires for Energy Conversion. *Chem. Rev.* **2010**, *110*, 527−546.

(20) Dong, Q. F.; Fang, Y. J.; Shao, Y. C.; Mulligan, P.; Qiu, J.; Cao, L.; Huang, J. S. Electron-Hole Diffusion Lengths > 175 μm in Solution-Grown Ch3nh3pbi3 Single Crystals. *Science* **2015**, *347*, 967−970.

(21) Liu, X.; Gu, L. L.; Zhang, Q. P.; Wu, J. Y.; Long, Y. Z.; Fan, Z. Y. All-Printable Band-Edge Modulated ZnO Nanowire Photodetectors with Ultra-High Detectivity. *Nat. Commun.* **2014**, *5*, 4007−4015.

(22) Li, Y. B.; Della Valle, F.; Simonnet, M.; Yamada, I.; Delaunay, J. J. High-Performance UV Detector Made of Ultra-Long ZnO Bridging Nanowires. *Nanotechnology* **2009**, *20*, 045501−045505.

(23) Soci, C.; Zhang, A.; Xiang, B.; Dayeh, S. A.; Aplin, D. P. R.; Park, J.; Bao, X. Y.; Lo, Y. H.; Wang, D. ZnO Nanowire UV Photodetectors with High Internal Gain. *Nano Lett.* **2007**, *7*, 1003−1009.

DOI: 10.1021/acsami.7b08066
ACS Appl. Mater. Interfaces 2017, 9, 31042−31053

(24) Lao, C. S.; Park, M. C.; Kuang, Q.; Deng, Y. L.; Sood, A. K.; Polla, D. L.; Wang, Z. L. Giant Enhancement in UV Response of ZnO Nanobelts by Polymer Surface-Functionalization. *J. Am. Chem. Soc.* **2007**, *129*, 12096−12097.
(25) Liu, K. W.; Sakurai, M.; Aono, M.; Shen, D. Z. Ultrahigh-Gain Single Sno2Microrod Photoconductor on Flexible Substrate with Fast Recovery Speed. *Adv. Funct. Mater.* **2015**, *25*, 3157−3163.
(26) Wang, H. B.; Gonzalez-Pedro, V.; Kubo, T.; Fabregat-Santiago, F.; Bisquert, J.; Sanehira, Y.; Nakazaki, J.; Segawa, H. Enhanced Carrier Transport Distance in Colloidal Pbs Quantum-Dot-Based Solar Cells Using ZnO Nanowires. *J. Phys. Chem. C* **2015**, *119*, 27265−27274.
(27) Gao, Y.; Wang, Z. L. Equilibrium Potential of Free Charge Carriers in a Bent Piezoelectric Semiconductive Nanowire. *Nano Lett.* **2009**, *9*, 1103−1110.
(28) Valdez, C. N.; Schimpf, A. M.; Gamelin, D. R.; Mayer, J. M. Proton-Controlled Reduction of ZnO Nanocrystals: Effects of Molecular Reductants, Cations, and Thermodynamic Limitations. *J. Am. Chem. Soc.* **2016**, *138*, 1377−1385.
(29) Lee, Y. J.; Ruby, D. S.; Peters, D. W.; McKenzie, B. B.; Hsu, J. W. P. ZnO Nanostructures as Efficient Antireflection Layers in Solar Cells. *Nano Lett.* **2008**, *8*, 1501−1505.
(30) Atwater, H. A.; Polman, A. Plasmonics for Improved Photovoltaic Devices. *Nat. Mater.* **2010**, *9*, 205−213.
(31) Liu, K. W.; Sakurai, M.; Liao, M. Y.; Aono, M. Giant Improvement of the Performance of ZnO Nanowire Photodetectors by Au Nanoparticles. *J. Phys. Chem. C* **2010**, *114*, 19835−19839.
(32) Gogurla, N.; Sinha, A. K.; Santra, S.; Manna, S.; Ray, S. K. Multifunctional Au-ZnO Plasmonic Nanostructures for Enhanced UV Photodetector and Room Temperature NO Sensing Devices. *Sci. Rep.* **2015**, *4*, 6483−6411.
(33) Wang, Z. L.; Wu, W. Z. Piezotronics and Piezo-phototronics: Fundamentals and Applications. *Natl. Sci. Rev.* **2014**, *1*, 62−90.
(34) Liu, Y.; Zhang, Y.; Yang, Q.; Niu, S. M.; Wang, Z. L. Fundamental Theories of Piezotronics and Piezo-phototronics. *Nano Energy* **2015**, *14*, 257−275.
(35) Wu, W. Z.; Pan, C. F.; Zhang, Y.; Wen, X. N.; Wang, Z. L. Piezotronics and Piezo-phototronics - From Single Nanodevices to Array of Devices and Then to Integrated Functional System. *Nano Today* **2013**, *8*, 619−642.
(36) Mandalapu, L. J.; Yang, Z.; Xiu, F. X.; Zhao, D. T.; Liu, J. L. Homojunction Photodiodes based on Sb-doped P-type ZnO for Ultraviolet Detection. *Appl. Phys. Lett.* **2006**, *88*, 383−385.
(37) Ni, P. N.; Shan, C. X.; Wang, S. P.; Li, B. H.; Zhang, Z. Z.; Zhao, D. X.; Liu, L.; Shen, D. Z. Enhanced Responsivity of Highly Spectrum-Selective Ultraviolet Photodetectors. *J. Phys. Chem. C* **2012**, *116*, 1350−1353.
(38) Kim, J.; Yun, J. H.; Kim, C. H.; Park, Y. C.; Woo, J. Y.; Park, J.; Lee, J. H.; Yi, J.; Han, C. S. ZnO Nanowire-Embedded Schottky Diode for Effective Uv Detection by the Barrier Reduction Effect. *Nanotechnology* **2010**, *21*, 115205−115209.
(39) Atwater, H. A.; Polman, A. Plasmonics for Improved Photovoltaic Devices (vol 9, pg 205, 2010). *Nat. Mater.* **2010**, *9*, 865−865.
(40) Hu, Y. F.; Chang, Y. L.; Fei, P.; Snyder, R. L.; Wang, Z. L. Designing the Electric Transport Characteristics of ZnO Micro/Nanowire Devices by Coupling Piezoelectric and Photoexcitation Effects. *ACS Nano* **2010**, *4*, 1234−1240.
(41) Zhu, L. H.; Gu, X. H.; Qu, F. D.; Zhang, J. Q.; Feng, C. H.; Zhou, J. R.; Ruan, S. P.; Kang, B. N. Electrospun ZnO Nanofibers-Based Ultraviolet Detector with High Responsivity. *J. Am. Ceram. Soc.* **2013**, *96*, 3183−3187.
(42) Yang, Q.; Guo, X.; Wang, W. H.; Zhang, Y.; Xu, S.; Lien, D. H.; Wang, Z. L. Enhancing Sensitivity of a Single ZnO Micro-/Nanowire Photodetector by Piezo-phototronic Effect. *ACS Nano* **2010**, *4*, 6285−6291.
(43) Harnack, O.; Pacholski, C.; Weller, H.; Yasuda, A.; Wessels, J. M. Rectifying Behavior of Electrically Aligned ZnO Nanorods. *Nano Lett.* **2003**, *3*, 1097−1101.
(44) Lao, C. S.; Liu, J.; Gao, P. X.; Zhang, L. Y.; Davidovic, D.; Tummala, R.; Wang, Z. L. ZnO Nanobelt/nanowire Schottky Diodes Formed by Dielectrophoresis Alignment Across Au Electrodes. *Nano Lett.* **2006**, *6*, 263−266.
(45) Fang, Y. J.; Dong, Q. F.; Shao, Y. C.; Yuan, Y. B.; Huang, J. S. Highly Narrowband Perovskite Single-Crystal Photodetectors Enabled by Surface-Charge Recombination. *Nat. Photonics* **2015**, *9*, 679−686.
(46) Fu, X. W.; Li, C. Z.; Fang, L.; Liu, D. M.; Xu, J.; Yu, D. P.; Liao, Z. M. Strain-Gradient Modulated Exciton Emission in Bent ZnO Wires Probed by Cathodoluminescence. *ACS Nano* **2016**, *10*, 11469−11474.
(47) Fu, X. W.; Liao, Z. M.; Liu, R.; Lin, F.; Xu, J.; Zhu, R.; Zhong, W.; Liu, Y. K.; Guo, W. L.; Yu, D. P. Strain Loading Mode Dependent Bandgap Deformation Potential in ZnO Micro/Nanowires. *ACS Nano* **2015**, *9*, 11960−11967.
(48) Liao, Z. M.; Wu, H. C.; Fu, Q.; Fu, X. W.; Zhu, X. L.; Xu, J.; Shvets, I. V.; Zhang, Z. H.; Guo, W. L.; Leprince-Wang, Y. M.; Zhao, Q.; Wu, X. S.; Yu, D. P. Strain Induced Exciton Fine-Structure Splitting and Shift in Bent ZnO Microwires. *Sci. Rep.* **2012**, *2*, 452−457.
(49) Guo, Z.; Zhao, D. X.; Liu, Y. C.; Shen, D. Z.; Zhang, J. Y.; Li, B. H. Visible and Ultraviolet Light Alternative Photodetector Based on ZnO Nanowire/N-Si Heterojunction. *Appl. Phys. Lett.* **2008**, *93*, 163501−163503.
(50) Konstantatos, G.; Badioli, M.; Gaudreau, L.; Osmond, J.; Bernechea, M.; de Arquer, F. P. G.; Gatti, F.; Koppens, F. H. L. Hybrid Graphene-Quantum Dot Phototransistors with Ultrahigh Gain. *Nat. Nanotechnol.* **2012**, *7*, 363−368.
(51) Ni, P. N.; Shan, C. X.; Wang, S. P.; Liu, X. Y.; Shen, D. Z. Self-Powered Spectrum-Selective Photodetectors Fabricated from N-Zno/P-Nio Core-Shell Nanowire Arrays. *J. Mater. Chem. C* **2013**, *1*, 4445−4449.

DOI: 10.1021/acsami.7b08066
ACS Appl. Mater. Interfaces 2017, 9, 31042−31053